*Pure Appl. Chem.*, Vol. 85, No. 7, pp. 1465–1478, 2013.
http://dx.doi.org/10.1351/PAC-CON-13-02-06


# Novel fluorescent probes based on intramolecular charge- and proton-transfer compounds*

Guoqiang Yang[1,‡], Shayu Li[1], Shuangqing Wang[1], Rui Hu[1], Jiao Feng[1], Yi Li[2], and Yan Qian[3]

*[1]Beijing National Laboratory for Molecular Sciences, Key Laboratory of Photochemistry, Institute of Chemistry, Chinese Academy of Sciences, Beijing 100190, China; [2]Key Laboratory of Photochemical Conversion and Optoelectronic Materials, Technical Institute of Physics and Chemistry, Chinese Academy of Sciences, Beijing 100190, China; [3]Key Laboratory for Organic Electronics and Information Displays and Institute of Advanced Materials, Nanjing University of Posts and Telecommunications, Nanjing, China*

*Abstract*: Excited-state intramolecular proton-transfer (ESIPT) compounds and intramolecular charge-transfer (ICT) compounds have attracted attention due to their interesting and even unique emission properties. The intense and environment-sensitive emission showed by some members of the two families has been exploited in fluorescent probes for various forms of environmental sensing. In this paper, we summarize our recent study on the utilization of novel ESIPT and ICT compounds with intense emission as fluorescent probes after an introduction to the ESIPT and/or ICT processes and related photophysics mechanism.

*Keywords*: aggregation-induced emission enhancement (AIEE); boron-containing compounds; excited-state intramolecular proton transfer (ESIPT); intramolecular charge transfer (ICT); luminescence; probes.

## INTRODUCTION

Luminescent compounds presently dominate the field of molecular probes for chemical analyses and bioassay because they offer advantages of high detection sensitivity, low background noise, and wide dynamic ranges [1]. These advantages will be particularly evident in the development of modern optical analytical equipment demanding high accuracy. Organic fluorescent compounds display high absorptivity and fluorescence quantum yields, which contributes to the reason that they are the most important family of luminescent probes. Dyes such as coumarin, cyanin, fluorescein, or rhodamine derivatives play a key role in commercial fluorescent labels owing to their easy modification and low cost [2]. Additionally, a number of boron-dipyrromethene (Bodipy) derivatives have been reported as luminescent probes since they show intense emission and narrow emission bands [3]. However, fluorescence of these common probes is often weakened or even quenched at high concentrations, which limits the effective ranges of their applications.

**Pure Appl. Chem.* **85**, 1257–1513 (2013). A collection of invited papers based on presentations at the XXIV[th] IUPAC Symposium on Photochemistry, Coimbra, Portugal, 15–20 July 2012.
‡Corresponding author

In the past decade, there has been growing interest in the development of excited-state intramolecular proton-transfer (ESIPT) compounds as probes for chemicals and biomolecules [4]. The main reason is probably that these compounds have unique and beneficial photophysical characteristics, such as unusually large Stokes shifts and outstanding environment-sensitive spectral changes [5]. It is well known that typical ESIPT molecules exist exclusively in an enolic form (E) in the ground state. Upon photoexcitation, extremely fast tautomerism from the excited enolic (E*) to the excited keto (K*) form occurs on a sub-picosecond time scale. After decay of K* to the ground state, the K form transforms to the initial E form through reverse proton transfer mediated by intramolecular hydrogen bonds. The different species between absorbing and emitting in the intrinsic four-level photocycle (E-E*-K*-K) offer a high probability to address the disadvantage of fluorescence concentration quenching that is suffered by almost all of the available luminescent probes. On the other hand, ESIPT involves a proton-transfer process that is easily affected by changes in surrounding conditions, leading to sensitive spectral responses. Naturally, various ESIPT structure centers (e.g., flavone, azole, benzazole, etc.) and substituent groups have been used to fabricate several luminescent probes that are utilized in sensing applications for polarity, pH, anions, and cations [6].

As another well-known adiabatic mechanism, intramolecular charge transfer (ICT) has been utilized to design fluorescent probes that display large Stokes shifts without self-reabsorption [7]. In general, the ICT process requires a conjugated system containing an electron donor moiety (amino, alkoxy, few sulfur-containing groups, etc.) and an electron acceptor moiety (cyano, carbonyl, or even π-system, etc.). In the ground state, ICT molecules exhibit relatively small CT characteristics (e.g., small dipole moment). Upon electronic excitation of ICT systems by light, an electronic redistribution that entails CT from donor to acceptor occurs, resulting in the transient alternation of excited-state properties. The energy difference between the lowest Franck–Condon excited state and the excited ICT state causes the desired large Stokes shifts. The significant changes of dipole moment render the CT emission with high sensitivity to the environment conditions, enabling the development of environment-sensitive luminescent probes. At present, applications of ICT compounds are growing in various probe fields [8].

The nature of the excited states of ESIPT and ICT dyes is more diverse than those of common organic luminophores, resulting in rich photophysical properties with high dependence on local environment. The intrinsic advantage of the large Stokes shifts makes these two classes of dyes ideal candidates for use as fluorescence probes. However, most ESIPT dyes exhibit low to very low fluorescence efficiency except for a few flavone- and imidazole-containing examples [9]. Furthermore, the fluorescence quantum yield of ICT emission is generally very low in a highly polar environment. Since weak fluorescence emission is detrimental to practical application, many efforts have been made to address the problem and develop novel intense luminescence probes. In the following section, we will summarize our recent works on the understanding of emission properties of the ESIPT and ICT molecules and how these properties are used to design desirable fluorescence probes.

## RESULTS AND DISCUSSION

### Aggregation-induced emission enhancement (AIEE) of the ESIPT compounds

Several research groups have reported very different organic systems with varying degrees of AIEE characteristic since Tang et al. found that a series of silole derivatives are non-emissive in dilute solutions but become highly luminescent in aggregate states [10]. Our research began with a typical ESIPT compound, *N*,*N*′-bis(salicylidene)-*p*-phenylenediamine (*p*-BSP) **1** [11]. *p*-BSP is a member of the salicylideneaniline (SA) family, which is known for photochromic properties [12]. The fluorescent quantum yield of *p*-BSP was only 0.001 in methanol solution, but the fluorescent intensity was impressively increased by more than 60 times when *p*-BSP was fabricated to nanoaggregates in water (Fig. 1). The relevant absorbance was red-shifted from 370 to 383 nm, suggesting the formation of *J*-aggregation or *J*-type stacking. The appearance of excitation spectra of the aggregates was very analogous to that of

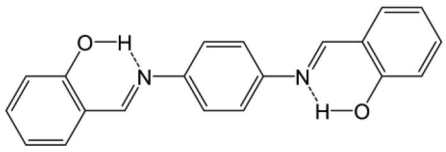

**1**

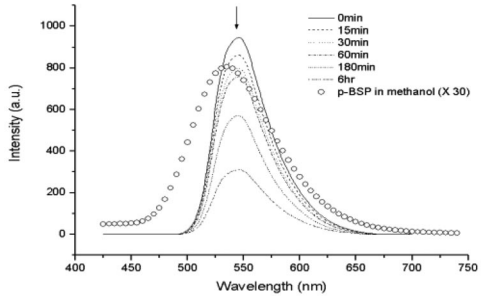


**Fig. 1** Fluorescence emission spectra of *p*-BSP nanoparticles ($1.0 \times 10^{-5}$ M in molecule) in water at different aging time and *p*-BSP in methanol solution ($1.0 \times 10^{-5}$ M, multiplied by a factor of 30). Reproduced from ref. [11], with permission of the American Chemical Society.

absorption spectra, indicating that the fluorescence originates from sole species. In the good solvents such as tetrahydrofuran (THF) and methanol, the *p*-BSP molecule should be nonplanar and may undergo some conformational changes. The two halves of the molecule were much less coupled due to the free rotation around the single bond. Upon addition of massive water, *p*-BSP molecules aggregated together due to their poor water solubility. Molecular mechanics force field computations with MM+ parametrization demonstrated that aggregation induced the planarization of *p*-BSP and restricted their rotations, which hampered the formation of radiationless photochromic species. Therefore, the enhanced emission of *p*-BSP was attributed to the combined effects of molecular planarization, restricted molecules rotations, together with *J*-aggregate formation. Considering that the red-shifts of absorbance were relatively small, the latter two may be the main factors for AIEE phenomenon.

The AIEE phenomenon of *p*-BSP is very impressive, but the fluorescent quantum efficiency (0.063) of aggregates is still not high enough for most luminescent applications. Moreover, the appearance of aggregates would change spontaneously from spherical to rod-like and finally to belt-like, accompanying the gradual decrease of fluorescent intensity. The relatively low fluorescent efficiency and the unstable structure limited potential practicality of the aggregates. Since the vibration and twist of the C=N bond would be the two most likely routes of nonradiate decay of *p*-BSP excited state, we developed two novel members of 2-(2'-hydroxyphenyl) benzothiazole-based (HBT-based) ESIPT compounds, *N*,*N*′-di[3-hydroxy-4-(2'-benzothiazole) phenyl] isophthalic amide (DHIA) **2** and *N*,*N*′-di[3-hydroxy-4-(2'-benzothiazole) phenyl] 5-*tert*-butyl-isophthalic amide (DHBIA) **3**, in which the C=N bond was fixed on the ring plane [13].

Both compounds were found to exhibit AIEE phenomena, which fluorescent efficiencies were increased from about 0.002 in THF solutions to 0.029 (DHIA) and 0.19 (DHBIA) in aggregates (Fig. 2), respectively. Whatever the case, the emission was always green originated from K* tautomer, while the emission from E* was so weak and considered negligible. Following our earlier studies on the AIEE phenomenon, the significant emission enhancement in aggregates was considered firstly as result of restriction of intramolecular rotations (RIR). In solution, the free rotation of end-substituted HBT units around the single bonds could effectively quench the excited states. While in the aggregate state, the

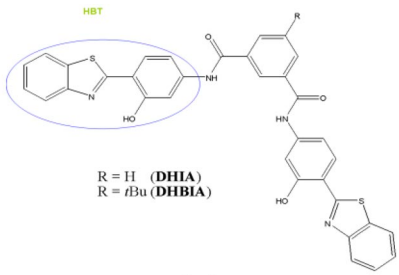


2, 3

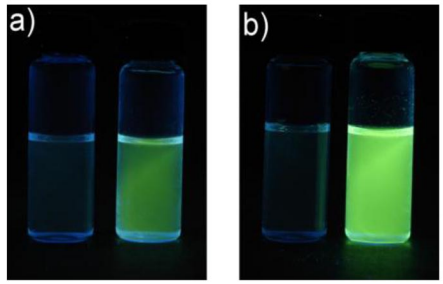


**Fig. 2** Photographs of DHIA (a) and DHBIA (b) with concentrations both of $5.0 \times 10^{-6}$ M in THF dilute solution (left) and in aggregates under irradiation at 365 nm. Reproduced from ref. [13], with permission of the American Chemical Society.

intramolecular rotation and torsion were greatly impeded and therefore the nonradiative decay channel was effectively restricted, which in turn populated the irradiative state of the excited molecules and resulted in a great increase of fluorescence. We noticed that the degrees of their fluorescence enhancement were quite different, while the AIEE of DHBIA was much more prominent. Since the structural difference between DHIA and DHBIA was only the substituent at the central ring of which orbit was not involved in the fluorescent state, there were other factors besides RIR that have impact on the AIEE phenomenon. The noteworthy discrimination of DHIA and DHBIA in the absorption spectra and their aggregate shapes allowed us to hypothesize that DHIA and DHBIA might present different aggregation modes. To minimize the total energy of the packing system, DHIA showed a parallel face-to-face H-aggregation with full π–π stacking as the primary alignment (Fig. 3a). The distances between molecules were 3.5 Å according to the molecular mechanics calculation, which was a common interval in planar aromatic system in crystal stacking. However, for DHBIA, the molecules were not able to possess an energy-favored full parallel π–π stacking but showed typical slip-stacking due to the steric restriction imposed by bulky *tert*-butyl groups (Fig. 3b). In this case, the distance between two HBT subunits of two adjacent molecules would be restrained at 3.4 Å, which indicated an intensified π–π stacking between the tail HBT arm of one molecule and the head HBT arm of another molecule. Meanwhile, the simulated result showed that the whole molecular structure became more planar in the stacking mode. In scanning electron microscopy (SEM) observations, the appearances of DHIA and DHBIA aggregates were cube- and rod-like, respectively. The growth tendency of two aggregates correlated well with their simulated aggregation fashions. After the investigation of the photophysical processes, the packing mode was found to affect the fluorescence efficiency as well as the ESIPT quantum efficiency. The ratios of inherent fluorescence efficiency of K* between aggregates and solution were similar in DHIA and DHBIA, indicating the similar effects of RIR. However, the ratio of quantum efficiency of ESIPT process depended on the packing mode. The H-aggregation in DHIA increased the internal conversion rate of the E* state, reducing the ESIPT efficiency, while for DHBIA, the reverse

 

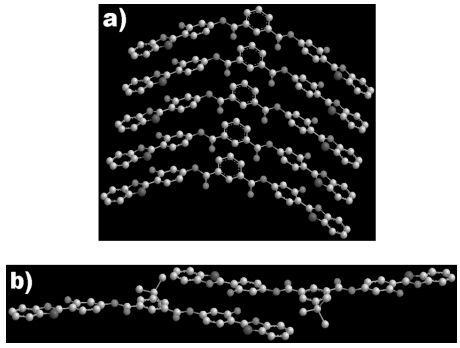


**Fig. 3** Simulated stacking modes of DHIA (a) and DHBIA (b) molecules utilizing π–π stacking of HBT subunits. Reproduced from ref. [13], with permission of the American Chemical Society.

was true. Since the total fluorescence efficiency was the product of ESIPT efficiency and inherent fluorescence efficiency of K*, the different degrees in their emission enhancement were caused by their different aggregation modes, which was only due to the steric effect of a single *tert*-butyl group substituted to the DHBIA molecule.

Subsequently, an ESIPT compound *N*-(4-(benzo[*d*]thiazol-2-yl)-3-hydroxyphenyl)-benzamide (BTHPB) 4 was synthesized to further understand the AIEE mechanism [14]. The chromophore moiety of BTHPB was the same as that of DHIA and DHBIA. The dilute solutions in organic solvents presented weak fluorescence, the quantum efficiency of which was just only 0.018. However, BTHPB showed apparent AIEE property and the emission efficiency was observed as high as 0.27 in the aggregates. The aggregates fluorescence energy and band shape were consistent with that of solution, suggesting that they came from the same excited state. The different quantum efficiency implied the different formation processes and/or radiationless decay routes of the excited states. Viscochromism experiments with mixtures of cyclohexane and paraffin oil demonstrated that the AIEE of BTHPB possibly originated from restriction of molecular torsions and rotations, e.g., RIR effect. According to the first-principles linear-coupling-model calculations, a reliable qualitative method to explore internal conversion nonradiative decay processes, the aromatic vibration and the rotation between the hydrobenzo[*d*]thiazole group and the cyclohexadienone ring that undertook the ESIPT process were the major radiationless decay routes (Fig. 4). In general, only molecular torsions and rotations but not vibrations were restrained effectively by tight packing of the molecules. Therefore, the restriction of molecular rotations should be the predominant factor of AIEE. Besides calculations, the micro- and femtosecond transient absorption experiments also offered evidence for consideration. In generally accepted ESIPT mechanism of HBT-type compounds, the excited state K* relaxed with two competitive processes: decay to the K ground state and nonradiative decay to the long-lifetime *trans*-keto photoproduct. Transient absorption measured with flash photolysis showed that *trans*-keto photoproduct of BTHPB with lifetime 500 μs only existed in solutions rather than in aggregates. The ultrafast absorption spectra also confirmed that the *trans*-keto photoproduct never formed after the ESIPT process when

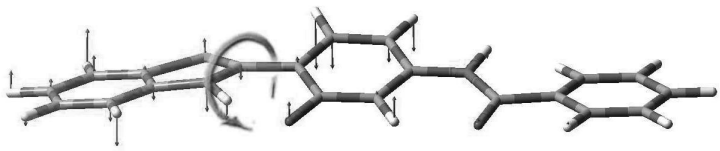

**Fig. 4** The scheme of major nonradiative decay route of BTHPB **4**. Reproduced from ref. [14], with permission of the Royal Society of Chemistry.

 

BTHPB molecule was restrained. The effects of aggregation on the fluorescence efficiency were not always promising; ESIPT efficiency in aggregates was only half of that in solution. The decrease probably resulted from the strong intermolecular interactions of the E forms in aggregates on account of the considerable changes of absorbance in the aggregates (Fig. 5). It indicated that the efficiency of the ESIPT process could not be simply assumed as 100 % and the total AIEE observation was the combination of the positive and negative aggregation effects. The results implied that designing luminescent compounds with higher emission efficiency in the solid (or aggregates) should be balanced by the intermolecular interactions.

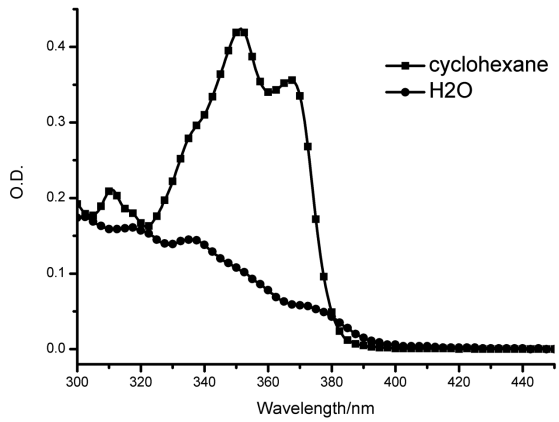


**Fig. 5** Absorption and fluorescence spectra of BTHPB in cyclohexane and water. Concentration: $1.0 \times 10^{-5}$ M. Excitation at 360 nm. Reproduced from ref. [14], with permission of the Royal Society of Chemistry.

## Fluorescence response of the ESIPT compounds

Since the proton-transfer process can be inhibited by an intermolecular hydrogen bond formed with surrounding molecules, the ESIPT process is generally sensitive to environments that contain proton donor and/or acceptor. Thus, the emission characteristics of ESIPT compounds are expected to be environment-dependent. Some ESIPT compounds may exhibit dual luminescence bands that can be adjusted with various solvents or even circumambient pressure, temperature conditions [15]. Also, different ESIPT molecules will have different responses to environmental elements. In principle, a molecule with more than one proton donor/acceptor pair should show a more profound emission nature with environmental change. We designed a novel triple-luminescence ESIPT compound *N*-salicylidene-3-hydroxy-4-(benzo[*d*]thiazol-2-yl) phenylamine (SalHBP) **5** containing two ESIPT subunits. SalHBP could emit blue or green or yellowish green or even nearly white light with conditions of various environment pressures, temperature, or different polarity solvent since its intramolecular hydrogen bond can be perturbed by surrounding factors [16].

The fluorescence spectra of SalHBP in meTHF at various pressures are shown in Fig. 6. At ambient pressure, the emission of SalHBP solutions was very weak and showed two peaks with maxima at 420 and 538 nm. Increasing pressure to about 5 kbar, the emission at 420 nm increased by almost ~3 times. Until the pressure increased to ~10 kbar, a new shoulder emission peak that could not be detected at ambient pressure was formed around 500 nm. This peak increased immediately after the pressure was enhanced and became obvious at 15.9 kbar and further increased until 31.2 kbar. With higher pressure up to 38.9 kbar, the peak around 538 nm increased significantly and the fluorescence of the ~500 nm peak prevailed. Note that the iso-emissive point around 530 nm was detected from 31.2 to 54.2 kbar, implying a conformational transition between two fluorescent species. On the basis of special structure, SalHBP molecules were expected to exhibit three possible emission bands. The three

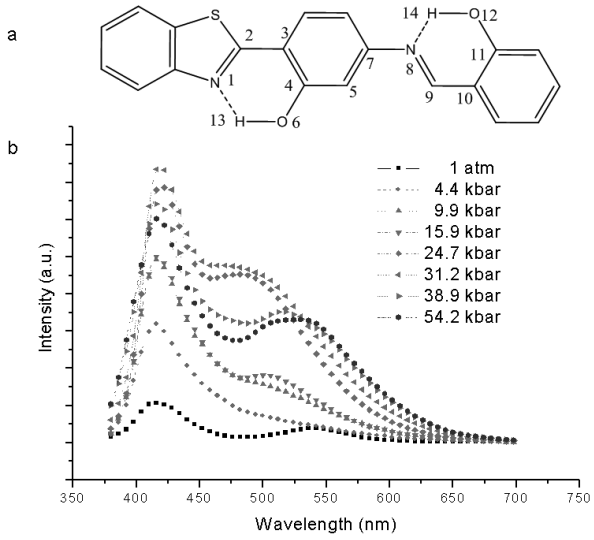


**Fig. 6** The fluorescence spectra of SalHBP in meTHF at various pressures. Reproduced from ref. [16a], with permission of the American Chemical Society.

emission bands around 420, 500, and 538 nm were assigned to enol-enol (EE), keto-enol (KE), and enol-keto (EK) characteristics. The assignments of these three emissions were confirmed by the analysis of emission and excitation spectra of the SalHBP solution. Since pressure would have a few effects on the ESIPT reaction rate, the response of EE luminescence to pressure was only correlated with the population of ESIPT reaction molecules. The essential condition for EE emission was the formation of intermolecular hydrogen bonds. The radial distribution function analysis of molecular dynamic simulations demonstrated that pressure reduced the intermolecular distances and increased the number of intermolecular hydrogen bonds. Because rotation and in-plane bending vibration were the most possible radiationless deactivation routes of KE tautomers according to the first-principles linear-coupling-model calculations, the increasing viscosity induced by pressure was the main reason for the KE emission enhancement with increasing pressure. The bending and stretching motions of bonds participated in the nonradiative decay process of EK tautomer. Because most of the bonds were located outside the molecule, pressure would restrict the bending motions and decreased internal conversion decay rate more or less. Additionally, increasing pressure would increase the population of molecules that could have ESIPT reaction to EK tautomer and decrease the probability that was from EE to KE tautomer simultaneously. The pressure-dependent, switchable colorful fluorescence made the SalHBP rather unique and possibly suitable for the important applications that include tristable switches and other optical devices (Fig. 7).

**Fig. 7** Photographs of SalHBP under 9.8 kbar (left), 25.2 kbar (middle), and 51.1 kbar (right). The diameter of the light spot is about 300 μm. Centers of light spot are overexposure. Reproduced from ref. [16a], with permission of the American Chemical Society.

 

The fluorescence spectra of SalHBP in various solvents are shown in Fig. 8. SalHBP exhibited a significant change in both fluorescence shape and intensity with different solvent environments. At ambient temperature, SalHBP showed two peaks with maxima at ~420 and ~538 nm in meTHF solution, but only one emission band at ~538 nm was observed in nonpolar MCH solution. Similarly, SalHBP also exhibited two emission bands in protic solvent methanol. But the emission in the high-energy area increased more than one order of magnitude compared to that of the meTHF solution. With decreasing temperature, the main emission band around 420 nm was enhanced only about 4-fold from 280 to 140 K in alcoholic mixture. Conversely, a remarkable increase of emission band at ~500 nm was observed when the temperature was below 180 K. In nonpolar MCH solution, SalHBP exhibited only a wide broad emission band, which maximum blue-shifted gradually from ~538 to ~500 nm with temperature decrease from 280 to 140 K. In the case of meTHF solution, SalHBP exhibited three emission bands with a peak at about 420, 500, and 538 nm at low temperature. According to the Car–Parrinello molecular dynamics simulations and time-dependent density functional theory calculations, three possible emission bands of SalHBP solutions could be obtained from five excited-state rotameric isomers. The luminescent color was determined by populations of the rotameric isomers. In protic solvent, the inter-inter EE2 was the main luminescent state due to strong intermolecular hydrogen-bonding formation with solvent molecules, leading to intense blue emission. In nonpolar solvent, intra-intra KE and EK rotamers were the most preferred ones, which resulted in the green emission with a wide band. In polar solvent, the relatively high polarity of solvent increased the population of conformations with large excited-state dipole moment, almost all rotamers were present in great population, activating all the three emission bands. As observed above, SalHBP presented apparent blue (CIE1931 0.20, 0.16), green (CIE1931 0.32, 0.46), and yellowish-green (CIE1931 0.33, 0.42) light in alcoholic, nonpolar and polar solutions, respectively, the luminescent color of which was temperature-independent. This compound provided a possible route for fabricating a white-light-emitting source with a single component luminescent material.

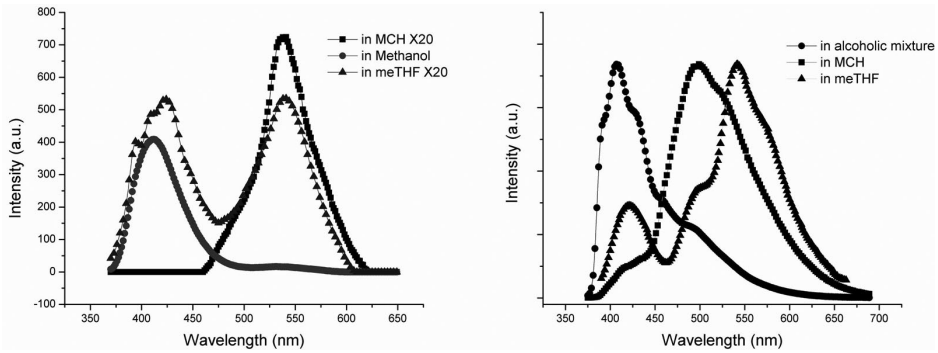


**Fig. 8** Normalized fluorescence emission spectra of SalHBP ($1.0 \times 10^{-5}$ M) in various solvents at room temperature (left) and 140 K (right). Excitation at 360 nm. Reproduced from ref. [16b], with permission of the American Chemical Society.

Figure 9 shows the colorful emission from SalHBP dispersed in copolymer (mole ratio of HEMA:VP 3:7), PS, and PMMA. A commercial UV-emissive light-emitting diode (LED) (365–375 nm) illuminated weak blue light. A thin transparent polymer layer was coated onto the LED head. Upon illumination, these LEDs generated white, bluish-green, and yellowish-green light, respectively. On the chromaticity diagram, these emissions showed Commission Internationale de L'Eclairage (CIE) coordinates at (0.29, 0.35), (0.26, 0.38), and (0.30, 0.42), in which the white emission was close to that of pure white light (0.33, 0.33). In PS, the case of SalHBP was similar to that in MCH where two intramoleculer hydrogen bonds of SalHBP exist most of the time, and the emission originated from two

ESIPT excited-state configurations and presented a green light for low polarity of PS. In PMMA, with higher polarity compared with MCH, PS, and meTHF, PMMA could increase the population of the tautomer with longer wavelength emission. So in PMMA, yellowish-green light was observed upon illumination. As SalHBP dissolved in HEMA-VP copolymer, the case was more complicated. Each excited-state conformation with different luminescence mentioned above was populated in the copolymer. This phenomenon was also explained by balance between intra- and intermolecular hydrogen bonds. Both HEMA and VP presented a great chance to form an intermolecular H-bond with dissolved SalHBP. But the possibility decreased when the monomer was polymerized to polymer for the limitation of free motion of the macromolecules. Suitable limitation resulted in a suitable population of the conformations with different color emission. By tuning the ratio of HEMA to VP in the copolymer, the coated LED generated pseudowhite light that was a combination of all emissions from several conformations of SalHBP, covering the whole visible range from 400 to 700 nm. Apparently, SalHBP can be considered as a potential luminescent material for environmental polarity detection.

## Fluorescent probe with the aggregates of the ESIPT compound

As mentioned previously, the ESIPT compounds show significant AIEE phenomenon. Their luminescence is closely correlated with populations of intra- and intermolecular hydrogen bonds that can easily be affected by the microenvironment. On the basis of our understanding of luminescence behaviors of the ESIPT compounds, we have developed a fluorescent probe that is capable of detecting fluoride ions in aqueous solution [17]. The sensor, which showed a high sensitivity, operated through the special affinity between fluoride ions and silicon, and provided two independent modes of signal transduction based on fluoride-dependent changes of fluorescence color (color metric mode) or intensity (power metric mode), respectively.

Fluoride anion, as the smallest anion, is an essential element in the human body and plays an important role in healthy and environmental issues, such as urolithiasis, fluorosis, and pollution of nuclear plants [18]. The U.S. Environmental Protection Agency (EPA) has set a maximum contaminant level (MCL) of 4 mg $L^{-1}$ (4 ppm) in drinking water. Considerable efforts have been devoted to design F-selective fluorescent probes [19]. Unfortunately, the incompatibility with aqueous environments is one of the main drawbacks that restrict the application of these probes. We chose an ESIPT compound *N*-(3-(benzo[*d*]thiazol-2-yl)-4-(hydroxyphenyl)benzamide (3-BTHPB) **6** and its silylated derivative *N*-(3-(benzo[*d*]thiazol-2-yl)-4-(*tert*-butyldiphenyl silyloxy)phenyl)-benzamide (BTTPB) **7** as probe dyes (Scheme 1).

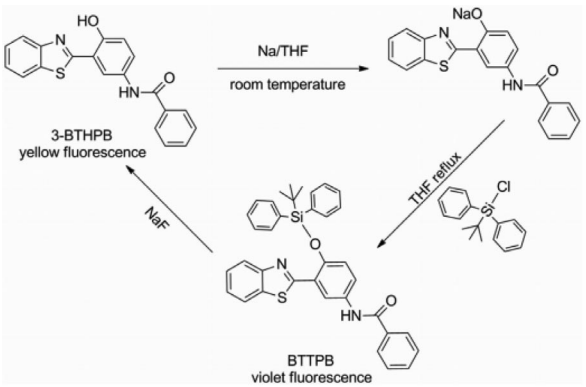


**Scheme 1** The synthesis of BTTPB, and the sensing mechanism of chemosensor BTTPB for detecting NaF. Reproduced from ref. [17], with permission of Wiley-VCH.

 

3-BTHPB showed two emission bands originated from the E and K forms at 418 and 560 nm, respectively. The ratio of the two bands was determined by the number of molecules that could undergo ESIPT reactions. However, only bright K-form yellow emission was observed in the aggregates. The BTTPB showed only blue–violet fluorescence, which was almost identical to the emission of the enol form of 3-BTHPB. With the aid of cetyltrimethylammonium bromide (CTAB) as a surfactant, BTTPB and 3-BTHPB, both of which were not soluble in water, were applied in aqueous environment. In 2 mM CTAB, BTTPB was in aggregated state and exhibited only one emission band with a maximum at 418 nm. Upon addition of fluoride ions, the blue–violet emission band decreased and a new emission band located at 560 nm simultaneously appeared and increased gradually, indicating the Si–O bond of BTTPB was immediately cleaved and 3-BTHPB was simultaneously released (Scheme 1). Furthermore, the combination of small micelle sizes and the mobility of organic molecules in the micelles made the interaction between BTTPB and fluoride ions facile. Addition of 0.95, 1.9, and 3.8 ppm of fluoride ions caused the dispersion fluorescence color to change from blue–violet to violet, pink–purple, and to pink–white, respectively. In color metric mode BTTPB/CTAB/water system was sufficiently sensitive for practical detection of fluoride ion in drinking water, standards of which are 1–4 ppm. With the selective excitation wavelength at 385 nm, BTTPB was nonfluorescent due to no absorbance at this wavelength, while the intensity of the yellow emission of 3-BTHPB increased drastically with fluoride ion concentration. The detection limit of the BTTPB dispersion system for fluoride ions was measured to be about 100 ppb. This result showed that in power metric mode the dispersion system had a very good sensitivity for the detection of aqueous fluoride ions. In both modes, the sensing process was rapid and took only 200 s, and offered excellent differentiation from other common anions such as $H_2PO_4^-$, $AcO^-$, or $NO_3^-$.

Fluorescence sensors for fluoride ion detection are usually solution-based. This approach is inconvenient since the sensors cannot be used as efficient tools under special circumstances, such as for in situ on-site detection. To facilitate the use of our system, we prepared test papers of BTTPB by immersing a filter paper in the solution of BTTPB in THF ($2.0 \times 10^{-3}$ M) and then drying it by exposure to air. For the detection of fluoride ions in water, the test paper was immersed in a fluoride-containing aqueous solution (containing 2 mM CTAB) and then exposed to air to remove water and to avoid further fluorescence color changes. The CIE 1931 ($x$,$y$) chromaticity diagram of the test papers after immersion in solutions of NaF with different concentrations for 3 min are shown in Fig. 10. Apparently, the easy-to-prepare test paper can be utilized to roughly and quantitatively detect and estimate the concentration of fluoride ions.

### Fluorescent temperature probe with the boron-containing ICT compound

ICT compounds have been widely used as fluorescent probes, but rare works exist to use ICT dye as a probe for local temperature. In general, the luminescence quantum yield of organic compounds decreases with increasing temperature due to the thermally induced radiationless transition [20]. Only a few compounds (Rhodamine 110, DMABN, PIPBN, etc.) exhibit a luminescence intensity maintenance or even an enhancement from lower temperature to room temperature [21]. The DMABN and PIPBN belong to the twisted ICT (TICT) compounds with dual fluorescence emission. The TICT process is concomitant with a luminescence colorimetric change that results from the shift of the thermal equilibrium between local excited-state emission (LE) and the TICT excited-state emission. However, it is difficult to apply the reported TICT compounds in thermal probe. Almost all TICT compounds have only moderate luminescent quantum yields and the luminescence decreases to very low levels at higher temperature, possibly resulting from free thermal vibrations of acceptor/donor subunits. Recently, several arylboron compounds were found to have high luminescence quantum yields, even above room temperature [22]. Three-coordinate boron is inherently electron-deficient and thus is a strong π-electron acceptor. In contrast to other strong π-acceptors such as the nitro group, the boron does not involve in the main nonradiative decay process. Therefore, a luminescent triarylboron mole-

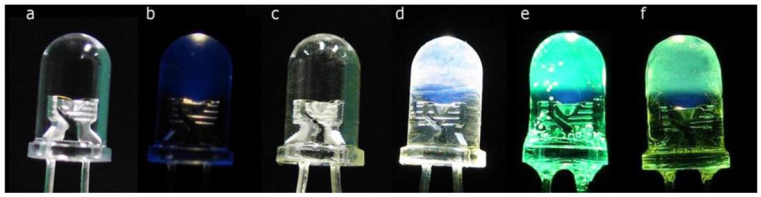


**Fig. 9** Photos of (a) a reference UV LED (365–375 nm) without illumination, (b) the illuminating reference LED, (c) the same LED coated with a thin layer of SalHBP HEMA-VP copolymer solution without illumination, (d) the illuminating LED shown in part c, (e) the same LED illuminating a coated thin layer of SalHBP PS solution, and (f) the same LED illuminating a coated thin layer of SalHBP PMMA solution. Reproduced from ref. [16b], with permission of the American Chemical Society.

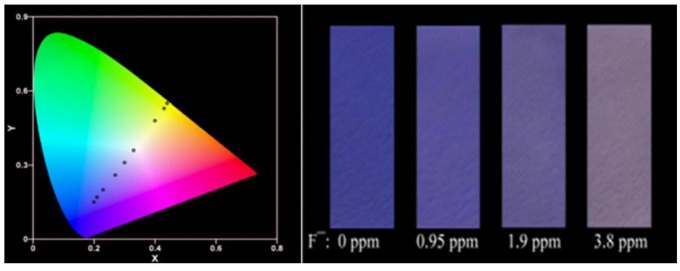


**Fig. 10** CIE 1931 (*x*,*y*) chromaticity diagram of the test paper for detecting NaF with different concentrations derived from fluorescence spectra. From left to right, NaF concentration: 0, 0.38, 0.95, 1.9, 3.8, 9.5, 19, 38, 95 ppm; and photos of the test papers after immersion into different concentrations of NaF. Reproduced from ref. [17], with permission of Wiley-VCH.

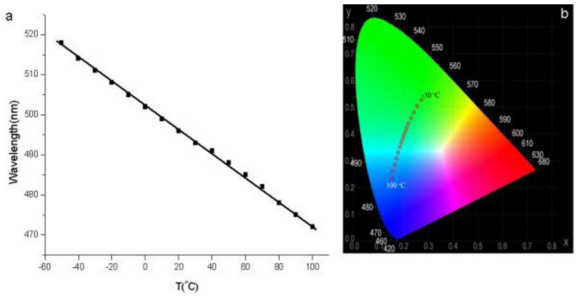


**Fig. 11** (a) Temperature dependence of maximum emission wavelength of DPTB; (b) CIE chromaticity diagram showing the temperature dependence of the (*x*,*y*) color coordinates of DPTB. Reproduced from ref. [23], with permission of Wiley-VCH.

cule, dipyren-1-yl (2,4,6-triisopropylphenyl) borane (DPTB) **8** was designed and synthesized for temperature probe [23].

DPTB shows temperature-dependent green-to-blue luminescence with a very high quantum yield (at least 0.64) over a wide temperature range (–50 to 100 °C) with high stability and reversibility in the solvent of 2-methoxyethyl ether (MOE). The corresponding wavelength shift per degree centigrade is as large as 0.30 nm, which can be readily measured by using a modern UV/vis fluorescence spectrometer, and is thus indicative of an accuracy better than 1 °C (Fig. 11a). The system color shifts can also be easily observed by the naked eye and captured by a single charge-coupled device (CCD) camera, the

accuracy is calculated to be approximately 2 °C (Fig. 11b). This intense thermosensitive emission over a wide range conquers the limitation that high temperatures induce a low signal/noise ratio, thus suggesting that DPTB is an excellent candidate for a reliable and absolute luminescent temperature probe. The mechanism for the thermosensitive emission was proposed. The DPTB exhibits an abnormally wide luminescence band that is identified as dual luminescence by its decay lifetime measurements. The components with shorter- and longer-wavelength luminescence bands are assigned to the emissions from the LE and TICT states of DPTB, respectively. Similar to the case of other dual-luminescent TICT compounds, the temperature strongly influenced the dynamic equilibrium between the LE and TICT excited states of DPTB. The luminescence color was determined by the population of two distinct excited-state conformations. The lower-energy TICT excited state is preferentially occupied with decreasing temperature, and, as expected a bathochromic shift of the luminescence is observed. Upon heating the system, the molecular motion that crosses the thermal barrier between the two excited states increases the population of the LE state, thus resulting in a hypsochromic luminescence. The applicability of this luminescent probe for detecting the temperature distribution in a certain area, as is often required in the automobile and aircraft industries, was examined. The DPTB–MOE solution was sealed in a sandwich structure PVC–porous PP–PVC film. The thickness of the film is 60 mm, making the film flexible and easy to adhere to the surface to map the temperature distribution. Considering the excited-state conformation changes in a time range of pico- or nanoseconds, the edge roughness of the pattern is only determined by the thermal diffusion coefficient of the conductive media. The edge roughness of the DPTB–MOE system is estimated to be 30–40 μm when the image capture time is set to 10 ms, indicative of a high spatial resolution. Therefore, the thin-film system containing DPTB–MOE can be used as a fluorescent probe for in situ large-area temperature measurement.

## CONCLUSIONS

Over the past few decades, many luminescent organic compounds have been exploited in the development of probes for the immediate surrounding environment. The ESIPT and ICT compounds have attracted much interest for the production of probe materials owing to their rich photophysical properties. Their intrinsically large Stokes shift addresses the problem of self-reabsorption and makes them attractive candidates for probe applications. To date, various approaches have been explored to improve their luminescent quantum efficiency. In this article, we summarized our efforts on understanding their photophysical processes and fabricating practical probes by taking their beneficial properties. The AIEE of ESIPT compounds was mainly caused by the restricted intramolecular motion as well as the larger population of intramolecular hydrogen bonds. The luminescence difference between intra- and intermolecular hydrogen-bond tautomers of ESIPT aggregate provided a selective and sensitive colorimetric route to detect fluoride anion in water. The visible colorful difference and high luminescence efficiency over a wide temperature range endowed the TICT boron-containing compound with the ability of surrounding temperature detection. To explore the potential of these compounds in probe application, it is necessary to undertake more basic photophysical research on related dyes with diverse forms, especially after we found that the different stacking modes were possibly responsible for different extents in the emission enhancement. Furthermore, in our continuing efforts to design and expand research, more luminescent ESIPT and ICT compounds with new functions will be discovered and used as sensors and probes for environments.

## ACKNOWLEDGMENTS

We are grateful for funding from the National Basic Research Program (2013CB834505, 2013CB834703, 2011CBA00905, and 2009CB930802) and the National Natural Science Foundation of China (21073206, 21072196, 21233011, and 21205122).

 

## REFERENCES


1. (a) A. Barbieri, G. Accorsi, N. Armaroli. *Chem. Commun.* 2185 (2008); (b) X. Q. Chen, X. Z. Tian, I. Shin, J. Yoon. *Chem. Soc. Rev.* **40**, 4783 (2011); (c) Z. M. Hudson, S. N. Wang. *Acc. Chem. Res.* **42**, 1584 (2009); (d) J. M. Klostranec, W. C. W. Chan. *Adv. Mater.* **18**, 1953 (2006); (e) K. K. W. Lo, C. K. Chung, N. Y. Zhu. *Chem.—Eur. J.* **12**, 1500 (2006); (f) E. G. Moore, A. P. S. Samuel, K. N. Raymond. *Acc. Chem. Res.* **42**, 542 (2009); (g) F. S. Richardson. *Chem. Rev.* **82**, 541 (1982).
2. (a) R. K. Emaus, R. Grunwald, J. J. Lemasters. *Biochim. Biophys. Acta* **850**, 436 (1986); (b) S. Salvioli, A. Ardizzoni, C. Franceschi, A. Cossarizza. *FEBS Lett.* **411**, 77 (1997); (c) C. T. Wittwer, M. G. Herrmann, A. A. Moss, R. P. Rasmussen. *Biotechniques* **22**, 130 (1997); (d) A. Pernthaler, C. M. Preston, J. Pernthaler, E. F. DeLong, R. Amann. *Appl. Environ. Microb.* **68**, 661 (2002); (e) N. C. Lim, J. V. Schuster, M. C. Porto, M. A. Tanudra, L. L. Yao, H. C. Freake, C. Bruckner. *Inorg. Chem.* **44**, 2018 (2005).
3. (a) Y. Gabe, Y. Urano, K. Kikuchi, H. Kojima, T. Nagano. *J. Am. Chem. Soc.* **126**, 3357 (2004); (b) R. Ziessel, G. Ulrich, A. Harriman. *New J. Chem.* **31**, 496 (2007); (c) G. Ulrich, R. Ziessel, A. Harriman. *Angew. Chem., Int. Ed.* **47**, 1184 (2008).
4. (a) A. D. Roshal, A. V. Grigorovich, A. O. Doroshenko, V. G. Pivovarenko, A. P. Demchenko. *J. Phys. Chem. A* **102**, 5907 (1998); (b) M. M. Henary, C. J. Fahrni. *J. Phys. Chem. A* **106**, 5210 (2002); (c) A. S. Klymchenko, A. P. Demchenko. *Phys. Chem. Chem. Phys.* **5**, 461 (2003); (d) M. M. Henary, Y. G. Wu, C. J. Fahrni. *Chem.—Eur. J.* **10**, 3015 (2004); (e) V. V. Shynkar, A. S. Klymchenko, C. Kunzelmann, G. Duportail, C. D. Muller, A. P. Demchenko, J. M. Freyssinet, Y. Mely. *J. Am. Chem. Soc.* **129**, 2187 (2007).
5. J. E. Kwon, S. Y. Park. *Adv. Mater.* **23**, 3615 (2011).
6. (a) H. Y. Luo, X. B. Zhang, C. L. He, G. L. Shen, R. Q. Yu. *Spectrochim. Acta A* **70**, 337 (2008); (b) W. H. Chen, Y. Xing, Y. Pang. *Org. Lett.* **13**, 1362 (2011); (c) C. C. Hsieh, P. T. Chou, C. W. Shih, W. T. Chuang, M. W. Chung, J. Lee, T. Joo. *J. Am. Chem. Soc.* **133**, 2932 (2011); (d) C. K. Lim, J. Seo, S. Kim, I. C. Kwon, C. H. Ahn, S. Y. Park. *Dyes Pigment* **90**, 284 (2011).
7. (a) W. Rettig.In *Topics in Current Chemistry, Electron Transfer I*, J. Mattay (Ed.), pp. 253–299, Springer, Berlin (1994); (b) K. Rurack. *Spectrochim. Acta A* **57**, 2161 (2001); (c) R. Badugu, J. R. Lakowicz, C. D. Geddes. *J. Am. Chem. Soc.* **127**, 3635 (2005); (d) M. Sameiro, T. Goncalves. *Chem. Rev.* **109**, 190 (2009); (e) X. Chen, Y. Zhou, X. J. Peng, J. Yoon. *Chem. Soc. Rev.* **39**, 2120 (2010).
8. (a) M. Maus, K. Rurack. *New J. Chem.* **24**, 677 (2000); (b) M. Sauer. *Angew. Chem., Int. Ed.* **42**, 1790 (2003); (c) Y. Suzuki, K. Yokoyama. *J. Am. Chem. Soc.* **127**, 17799 (2005); (d) M. E. Vazquez, J. B. Blanco, B. Imperiali. *J. Am. Chem. Soc.* **127**, 1300 (2005); (e) N. Shao, J. Y. Jin, H. Wang, Y. Zhang, R. H. Yang, W. H. Chan. *Anal. Chem.* **80**, 3466 (2008); (f) R. Hanf, S. Fey, B. Dietzek, M. Schmitt, C. Reinbothe, S. Reinbothe, G. Hermann, J. Popp. *J. Phys. Chem. A* **115**, 7873 (2011).
9. (a) P. T. Chou, M. L. Martinez. *Radiat. Phys. Chem.* **41**, 373 (1993); (b) S. Park, O. H. Kwon, S. Kim, M. G. Choi, M. Cha, S. Y. Park, D. J. Jang. *J. Am. Chem. Soc.* **127**, 10070 (2005).
10. (a) J. D. Luo, Z. L. Xie, J. W. Y. Lam, L. Cheng, H. Y. Chen, C. F. Qiu, H. S. Kwok, X. W. Zhan, Y. Q. Liu, D. B. Zhu, B. Z. Tang. *Chem. Commun.* 1740 (2001); (b) J. W. Chen, B. Xu, X. Y. Ouyang, B. Z. Tang, Y. Cao. *J. Phys. Chem. A* **108**, 7522 (2004); (c) A. J. Qin, C. K. W. Jim, Y. H. Tang, J. W. Y. Lam, J. Z. Liu, F. Mahtab, P. Gao, B. Z. Tang. *J. Phys. Chem. B* **112**, 9281 (2008); (d) B. K. An, J. Gierschner, S. Y. Park. *Acc. Chem. Res.* **45**, 544 (2012); (e) C. T. Lai, J. L. Hong. *J. Mater. Chem.* **22**, 9546 (2012); (f) J. Mei, Y. J. Wang, J. Q. Tong, J. Wang, A. J. Qin, J. Z. Sun, B. Z. Tang. *Chem.—Eur. J.* **19**, 612 (2013).
11. S. Y. Li, L. M. He, F. Xiong, Y. Li, G. Q. Yang. *J. Phys. Chem. B* **108**, 10887 (2004).


 

12. M. Ziółek, J. Kubicki, A. Maciejewski, R. Naskręcki, A. Grabowska. *Chem. Phys. Lett.* **369**, 80 (2003).
13. Y. Qian, S. Y. Li, G. Q. Zhang, Q. Wang, S. Q. Wang, H. J. Xu, C. Z. Li, Y. Li, G. Q. Yang. *J. Phys. Chem. B* **111**, 5861 (2007).
14. R. Hu, S. Y. Li, Y. Zeng, J. P. Chen, S. Q. Wang, Y. Li, G. Q. Yang. *Phys. Chem. Chem. Phys.* **13**, 2044 (2011).
15. (a) S. Santra, G. Krishnamoorthy, S. K. Dogra. *Chem. Phys. Lett.* **311**, 55 (1999); (b) A. O. Doroshenko, E. A. Posokhov, A. A. Verezubova, L. M. Ptyagina. *J. Phys. Org. Chem.* **13**, 253 (2000); (c) A. S. Klymchenko, V. G. Pivovarenko, T. Ozturk, A. P. Demchenko. *New J. Chem.* **27**, 1336 (2003); (d) P. T. Chou, C. H. Huang, S. C. Pu, Y. M. Cheng, Y. H. Liu, Y. Wang, C. T. Chen. *J. Phys. Chem. A* **108**, 6452 (2004); (e) P. T. Chou, W. S. Yu, Y. M. Cheng, S. C. Pu, Y. C. Yu, Y. C. Lin, C. H. Huang, C. T. Chen. *J. Phys. Chem. A* **108**, 6487 (2004); (f) A. S. Klymchenko, H. Stoeckel, K. Takeda, Y. Mely. *J. Phys. Chem. B* **110**, 13624 (2006).
16. (a) S. Y. Li, Q. Wang, Y. Qian, S. Q. Wang, Y. Li, G. Q. Yang. *J. Phys. Chem. A* **111**, 11793 (2007); (b) W. H. Sun, S. Y. Li, R. Hu, Y. Qian, S. Q. Wang, G. Q. Yang. *J. Phys. Chem. A* **113**, 5888 (2009).
17. R. Hu, J. A. Feng, D. H. Hu, S. Q. Wang, S. Y. Li, Y. Li, G. Q. Yang. *Angew. Chem., Int. Ed.* **49**, 4915 (2010).
18. (a) B. G. Shah, K. D. Trick, B. Belonje. *Trace Elem. Med.* **8**, 154 (1991); (b) M. S. McDonagh, P. F. Whiting, P. M. Wilson, A. J. Sutton, I. Chestnutt, J. Cooper, K. Misso, M. Bradley, E. Treasure, J. Kleijnen. *Brit. Med. J.* **321**, 855 (2000); (c) P. P. Singh, M. K. Barjatiya, S. Dhing, R. Bhatnagar, S. Kothari, V. Dhar. *Urol. Res.* **29**, 238 (2001); (d) M. S. Onyango, Y. Kojima, O. Aoyi, E. C. Bernardo, H. Matsuda. *J. Colloid Interface Sci.* **279**, 341 (2004); (e) S. Ayoob, A. K. Gupta. *Crit. Rev. Environ. Sci. Technol.* **36**, 433 (2006); (f) N. A. Anderson, P. Sabharwall. *Nucl. Technol.* **178**, 335 (2012).
19. (a) N. DiCesare, J. R. Lakowicz. *Anal. Biochem.* **301**, 111 (2002); (b) Y. Kubo, M. Yamamoto, M. Ikeda, M. Takeuchi, S. Shinkai, S. Yamaguchi, K. Tamao. *Angew. Chem., Int. Ed.* **42**, 2036 (2003); (c) M. Vazquez, L. Fabbrizzi, A. Taglietti, R. M. Pedrido, A. M. Gonzalez-Noya, M. R. Bermejo. *Angew. Chem., Int. Ed.* **43**, 1962 (2004); (d) R. Badugu, J. R. Lakowicz, C. D. Geddes. *Sens. Actuators, B* **104**, 103 (2005); (e) B. Liu, H. Tian. *J. Mater. Chem.* **15**, 2681 (2005); (f) T. W. Hudnall, F. P. Gabbai. *Chem. Commun.* 4596 (2008); (g) S. Kumar, V. Luxami, A. Kumar. *Org. Lett.* **10**, 5549 (2008); (h) R. M. Duke, E. B. Veale, F. M. Pfeffer, P. E. Kruger, T. Gunnlaugsson. *Chem. Soc. Rev.* **39**, 3936 (2010).
20. M. Gouterman. *J. Chem. Phys.* **36**, 2846 (1962).
21. (a) M. Vanderauweraer, Z. R. Grabowski, W. Rettig. *J. Phys. Chem.* **95**, 2083 (1991); (b) C. Cornelissen-Gude, W. Rettig. *J. Phys. Chem. A* **102**, 7754 (1998); (c) J. Sakakibara, R. J. Adrian. *Exp. Fluids* **26**, 7 (1999).
22. (a) D. R. Bai, X. Y. Liu, S. I. Wang. *Chem.—Eur. J.* **13**, 5713 (2007); (b) Z. M. Hudson, S. B. Zhao, R. Y. Wang, S. N. Wang. *Chem.—Eur. J.* **15**, 6131 (2009); (c) Z. M. Hudson, S. N. Wang. *Dalton Trans.* **40**, 7805 (2011).
23. J. Feng, K. J. Tian, D. H. Hu, S. Q. Wang, S. Y. Li, Y. Zeng, Y. Li, G. Q. Yang. *Angew. Chem., Int. Ed.* **50**, 8072 (2011).

 